

Journal of Materials Chemistry A

Accepted Manuscript



This is an *Accepted Manuscript*, which has been through the Royal Society of Chemistry peer review process and has been accepted for publication.

Accepted Manuscripts are published online shortly after acceptance, before technical editing, formatting and proof reading. Using this free service, authors can make their results available to the community, in citable form, before we publish the edited article. We will replace this *Accepted Manuscript* with the edited and formatted *Advance Article* as soon as it is available.

You can find more information about *Accepted Manuscripts* in the [Information for Authors](#).

Please note that technical editing may introduce minor changes to the text and/or graphics, which may alter content. The journal's standard [Terms & Conditions](#) and the [Ethical guidelines](#) still apply. In no event shall the Royal Society of Chemistry be held responsible for any errors or omissions in this *Accepted Manuscript* or any consequences arising from the use of any information it contains.



Journal Name

ARTICLE

Mechanical Properties of Organic-Inorganic Halide Perovskites, $\text{CH}_3\text{NH}_3\text{PbX}_3$ (X=I, Br and Cl), by Nanoindentation

Shijing Sun,^a Yanan Fang,^b Gregor Kieslich,^a Tim J. White^{*b} and Anthony K. Cheetham^{*a}

Received 00th January 20xx,
Accepted 00th January 20xx

DOI: 10.1039/x0xx00000x

www.rsc.org/

We report an experimental study of the mechanical properties of the organic-inorganic halide perovskites, $\text{CH}_3\text{NH}_3\text{PbX}_3$ (X=I, Br and Cl). Nanoindentation on single crystals was used to obtain Young's moduli (E) and hardnesses (H) of this class of hybrid materials, which have attracted considerable attention for photovoltaic applications. The measured Young's moduli of this family lie in the range 10-20 GPa and a trend of $E_{\text{Cl}} > E_{\text{Br}} > E_{\text{I}}$ is observed. The physical properties are consistent with the underlying crystal structure. In particular, the results are in reasonable agreement with recent calculations using density functional theory and align with expectations based upon bond energy, packing, and hydrogen-bonding considerations. The anisotropy in these systems is quite small, with $E_{100} > E_{110}$ for the cubic bromide and chloride cases and $E_{112} \approx E_{100}$ for the tetragonal iodide perovskites. Interestingly, $\text{CH}_3\text{NH}_3\text{PbI}_3$ is harder than the Br- and Cl-based perovskites.

Introduction

As a new class of promising photovoltaic materials, organic-inorganic halide perovskites have recently led to a remarkable breakthrough in the field of solar cell research. The solar-to-electrical power conversion efficiencies of $\text{CH}_3\text{NH}_3\text{PbX}_3$ (X=I, Br and Cl) has soared from 3.8% in 2009¹ to exceed 20% now under laboratory conditions.² Current research focuses on the controlled tuning of materials composition, film morphology and device design, in order to understand the mechanism of charge transport and further enhance the turn-over efficiencies of these perovskite-based solar cells.³⁻¹³ The extraordinary performance of this family of hybrid perovskites has been attributed to their large absorption coefficients, long-range electron-hole transport lengths, as well as their high charge carrier mobilities.^{3,5,9} The materials benefit further from scalable solution processing methods and have also shown promising potential in areas such as light emitting diodes, field effect transistors and solar thermoelectric applications.^{8,11,14} As the investigations of perovskite thin film technology continue, single crystals have attracted increasing attention due to their high diffusion lengths compared with polycrystalline thin films, which is critical for achieving high

efficiencies.^{15,16}

There has been rapid progress in the study of the physical properties and electronic structures of these hybrid perovskites,^{3,12,17-19} but no experimental investigations of their mechanical properties have been reported. There is concern that their application in devices may be limited by their lack of robustness, thermal stability and low electrical conductivity compared to inorganic materials.²⁰ In particular, the stress state and the crystallinity of the perovskite-layer have a strong impact on the absorption performance. *Feng et al.* reported first-principles calculations on the structural, elastic and anisotropic properties of the lead and tin based bromide and iodide systems.²¹ However, the measurement of the elastic and plastic responses of organic-inorganic hybrid materials is challenging since high sample quality and novel characterization techniques are required. Recent developments of the nanoindentation technique, wherein load and depth of penetration can be measured with resolution of 1 nN and 0.2 nm, respectively, have facilitated the quantitative characterization of the mechanical properties of a range of crystalline hybrid frameworks.²² For example, recent work on the structurally related amine formate perovskites, $[\text{AmineH}^+][\text{M}(\text{HCOO})_3]$, where M is a divalent transition metal, include studies of mechanical properties by single crystal nanoindentation techniques.^{23,24} In this family, the hydrogen-bonding interactions between the protonated amine and the formate framework crucially influence the elastic responses.

In the present study we report the mechanical properties of single crystals of the halide perovskites, $\text{CH}_3\text{NH}_3\text{PbX}_3$ (X=I, Br and Cl), using nanoindentation techniques. The elastic and

^a Department of Materials Science & Metallurgy, University of Cambridge, 27 Charles Babbage Road, Cambridge, CB3 0FS. E-mail: akc30@cam.ac.uk

^b School of Materials Science and Engineering, Nanyang Technological University, 50 Nanyang Avenue, Singapore, 639798. Email: tjwhite@ntu.edu.sg

* Electronic Supplementary Information (ESI) available: Hardness plot as a function of indentation depth, a summarised results table and nanoindentation details are presented. See DOI: 10.1039/x0xx00000x

plastic responses are measured along different crystallographic directions and the anisotropy of the properties is investigated. The study yields insight into the intrinsic properties of these hybrid lead halides materials and their underlying structure-property relationships.

Experimental

Synthesis

Single crystals of $\text{CH}_3\text{NH}_3\text{PbX}_3$ ($X=\text{I}, \text{Br}$ and Cl) were prepared by precipitation from hydrochloric, hydrobromic and hydroiodic acid solutions after the method of Poglitsch et al.²⁵ In this procedure, 2.5 g lead(II) acetate (Chemical Reagents, Sigma-Aldrich) was dissolved in 10 ml of concentrated aqueous HCl (37 wt%)/ HBr (48 wt%)/ HI (57 wt%) and heated to above 90°C . To this solution, 2 ml of concentrated HX ($X = \text{Cl}, \text{Br}$ and I) was added together with 0.597 g of CH_3NH_2 (40wt% aqueous solution, Merck). Crystals about 2 mm in dimension were obtained by cooling the solutions from $\sim 90^\circ\text{C}$ to 25°C over 72 hours. The products were colourless for the chloride, orange for the bromide and black for the iodide (Fig. 1). For $\text{CH}_3\text{NH}_3\text{PbI}_3$, the crystals were separated at above 40°C to avoid the formation of yellow crystalline $(\text{CH}_3\text{NH}_3)_4\text{PbI}_6 \cdot 2\text{H}_2\text{O}$.²⁶

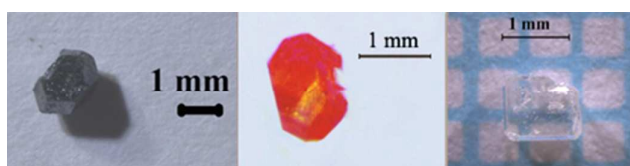


Fig. 1 Representative single crystals of $\text{CH}_3\text{NH}_3\text{PbI}_3$, $\text{CH}_3\text{NH}_3\text{PbBr}_3$, and $\text{CH}_3\text{NH}_3\text{PbCl}_3$ (from left to right).

Nanoindentation

In a first step, face indexing was carried out by single crystal X-ray diffraction using an Oxford Diffraction Gemini E Ultra diffractometer with Mo K_α radiation, $\lambda=0.7093 \text{ \AA}$, at 297 K (see Fig.S1). Favourable facets of the crystals, in particular the $\{100\}$ and $\{110\}$ planes from cubic Br and Cl-based perovskites and $\{100\}$ and $\{112\}$ planes from the tetragonal I-based perovskites, were identified. In terms of surface area requirements for sample preparation,²²⁻²⁴ these were the only high symmetry facets suitable for nanoindentation. Crystals were then selected and cold-mounted in Epofix resin (Struers Ltd.). Each individually indexed crystal surface was carefully polished with increasingly fine diamond suspensions to minimize surface roughness and nanoindentation experiments were conducted immediately after polishing to avoid sample degradation over time. Nanoindentation was performed at room temperature with the indenter aligned normal to the indexed facets using an MTS NanoIndenter[®] XP (MTS Corp., Eden Prairie, MN).^{23,27} Thermal instability and acoustic interference were minimized by keeping the instrument in an isolation cabinet. In the continuous stiffness measurement (CSM) mode, where indentation is controlled by displacement,

the Young's modulus (E) and hardness (H) were measured using a three-sided, sharp pyramidal Berkovich diamond tip (tip radius $\sim 100 \text{ nm}$).^{28,29} Mechanical responses were deduced from load-displacement (P - h) data according to the method of Oliver and Pharr.^{30,31}

Results and Discussion

Nanoindentation provides a reliable way of probing the anisotropic mechanical behaviour since the measured stiffness is strongly dependent on the elastic response along the indenter axis and only weakly affected transversely.^{27,32} Young's moduli and hardness values of the methylammonium lead halide crystals averaged from surface penetration depths between 200 nm and 1000 nm are presented in Table 1 (further details are given in the S.I.). The overall results reveal that, at room temperature, the elastic moduli of $\text{CH}_3\text{NH}_3\text{PbX}_3$ ($X=\text{I}, \text{Br}$ and Cl) single crystals vary in the range 10-20 GPa and a general trend of $E_{\text{Cl}} > E_{\text{Br}} > E_{\text{I}}$ is observed. In addition, E_{100} is greater than E_{110} for the cubic bromide and chloride cases.

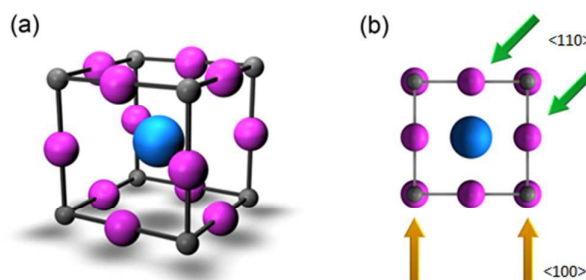


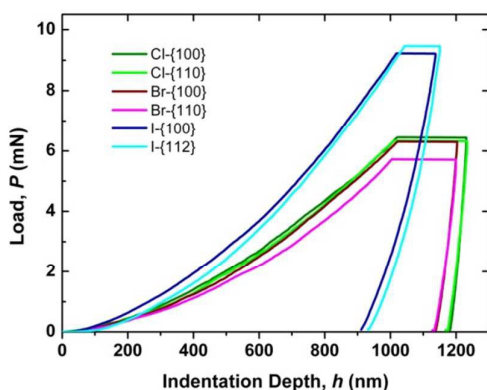
Fig. 2 (a) Idealised representation of the perovskite crystal structure of $\text{CH}_3\text{NH}_3\text{PbX}_3$ ($X=\text{I}, \text{Br}$ and Cl), (b) Illustration of nanoindentation along $\langle 100 \rangle$ (yellow arrows) and $\langle 110 \rangle$ (green arrows) directions in a cubic phase crystal. The grey spheres represent lead ions, purple spheres represent halogen ions and blue spheres represent the methylammonium ions.

As shown in Fig. 2, the measured mechanical anisotropy within each halide system can be linked to the underlying crystal structure. Along $\langle 100 \rangle$ directions of the cubic perovskite crystals, the indentation was aligned with the Pb-X-Pb inorganic direction, hence there is a strong resistance from the inorganic bonds. When the stress pushes along the $\langle 110 \rangle$ direction in the cubic system, the indenter moves against the face diagonal of the inorganic lattice, which is less rigid and generates more displacement, in agreement with the experimental results of lower moduli. At room temperature, the Br- and Cl-based perovskites are cubic whereas the I-based perovskite adopts tetragonal symmetry with a phase transition from tetragonal to cubic at around 57°C .³³ For the I-based perovskites, nanoindentation on the $\{100\}$ and $\{112\}$ facets reveal similar values for the Young's modulus since these are equivalent to $\{101\}$ and $\{110\}$ in a cubic cell. No other facets were found suitable for the nanoindentation experiment. In the tetragonal structure, a tilting of the PbI_6 octahedra of 16.4° at 293K , as well as a ferroelectric off-centring along the c -axis,

Table 1 Experimental and theoretical values of the elastic modulus and hardness anisotropy of the $\text{CH}_3\text{NH}_3\text{PbX}_3$ ($X=\text{I}, \text{Br}$ and Cl) perovskites.

Composition	Phase	Orientation	Young's Modulus (E) /GPa	Theoretical Modulus (E) /GPa ²¹	Hardness (H) /GPa
$\text{CH}_3\text{NH}_3\text{PbI}_3$	Tetragonal	{100}*	10.4(8)	Tetragonal Phase - 12.8 GPa	0.42(4)
	Tetragonal	{112}*	10.7(5)	Cubic Phase - 22.2 GPa	0.46(6)
$\text{CH}_3\text{NH}_3\text{PbBr}_3$	Cubic	{100}	17.7(6)	Tetragonal Phase - 15.1 GPa	0.31(2)
	Cubic	{110}	15.6(6)	Cubic Phase - 29.1 GPa	0.26(2)
$\text{CH}_3\text{NH}_3\text{PbCl}_3$	Cubic	{100}	19.8(7)	No values reported	0.29(2)
	Cubic	{110}	17.4(7)		0.25(2)

*The {100} and {112} planes in a tetragonal lattice are parallel to {110} and {101} planes, respectively, in the case of a cubic lattice.

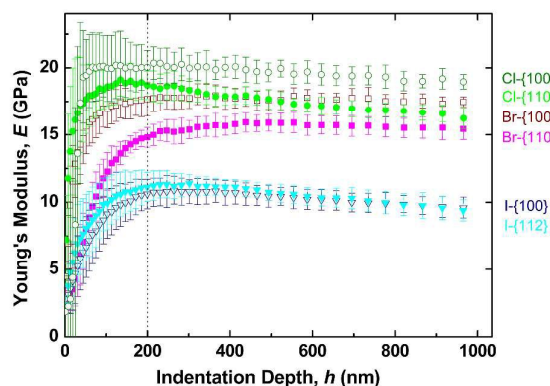
**Fig. 3** Typical load-displacement curves of different facets of $\text{CH}_3\text{NH}_3\text{PbX}_3$ ($X=\text{I}, \text{Br}$ and Cl).

have been observed.³⁴ The tilting of the polyhedra might lead us to expect less anisotropy in the Young's modulus than for the chloride and bromide because the Pb-I-Pb chains are no longer linear. Unfortunately, we were unable to observe this effect due to the absence of suitable crystal facets.

Typical load-displacement (P - h) curves are presented to show the stress states of $\text{CH}_3\text{NH}_3\text{PbX}_3$ ($X = \text{Cl}, \text{Br}, \text{I}$) as the indenter penetrates the sample surfaces (Fig. 3). The gradient of the initial unloading sections of the P - h curves provides an indication of the elastic moduli. During unloading, an elastically strained material relaxes back to its original shape; however, the presence of the plastic zone leads to a residual impression on the sample surface after the load is completely removed.^{24,35} All the P - h plots, especially for the Br and Cl-based perovskites, exhibit large residual depths from unloading, indicating that significant plastic deformation occurred underneath the Berkovich tip. The organic-inorganic halide perovskites may therefore potentially be able to facilitate applications in compliant devices that demand plastic deformations. The I-based perovskites, however, show better elastic recovery, indicated by the smaller residue displacement after unloading. The loading segments of the P - h curves obtained from all crystals are smooth, and the absence of discontinuities ("pop-in" events) indicates that there were no

heterogeneous deformations during indentation. Nor were any stress-induced phase transformations observed.²⁷

The elastic moduli averaged over 10-20 indentations on each crystal (variations are due to differences in crystal sizes) are plotted as a function of indentation depth for each facet in Fig. 4. The experimental results are in reasonable agreement with the theoretical calculations on the mechanical properties (Table 1).²¹ I-based perovskites show very good consistency with calculations for the tetragonal system. For Br-based perovskite, however, although the crystals were cubic, the measured Young's Modulus is closer to the theoretical predictions for the tetragonal phase. In addition, our results for the Young's modulus are consistent with the theoretical calculations of the bulk modulus by Giorgi et. al., where a trend of $\text{Cl} > \text{Br} > \text{I}$ was also observed.³⁶

**Fig. 4** Elastic moduli averaged over at least 10 indents on each crystal as a function of the indentation depth.

In order to understand the trend in mechanical response in terms of the bonding within the different structures, we now discuss three chemical factors that might influence the mechanical behaviour of these hybrid perovskites: (i) the Pb-X bond strengths, (ii) the packing density, and (iii) hydrogen-bonding between the CH_3NH_3^+ cations and the halide anions. The Pb-X chemical bonding is believed to be an important factor in determining the physical properties of the lead halides.³⁷ As shown in Fig. 5 (a),³⁸ the increasing Pb-X bond

strengths in the sequence $E_I < E_{Br} < E_{Cl}$ correlates well with the increasing Young's moduli. Secondly, the relative packing densities should also influence the mechanical properties, and here we use the Goldschmidt's tolerance factor $\alpha = (r_{A,eff.} + r_X) / \sqrt{2}(r_B + r_X)$, where r_i is the radius of the ion of the i site of perovskite structure, with $i = A, B$ and X , respectively, to reflect the trend in packing densities.^{39,40} In this approach, protonated amines are treated as spheres with a semi-empirical radius, $r_{A,eff.}$ ⁴¹ The effective radius of the methylammonium ion at the A site has been estimated as $r_{A,eff.} = 217$ pm. The tolerance factors for $\text{CH}_3\text{NH}_3\text{PbX}_3$ ($X = \text{Cl}, \text{Br}, \text{I}$) are hence calculated as Cl: 0.94, Br: 0.93, and I: 0.91, respectively.⁴¹ Fig. 5(b) reveals that the packing densities, as represented by the tolerance factors, correlate nicely with the Young's moduli, suggesting that the more densely packed structures are more resilient to elastic deformation.

Hydrogen-bonding interactions between the A-site cation and the framework are known to have a strong influence on the mechanical properties of metal-organic formate perovskites,^{23,24} and recent DFT calculations on the orthorhombic phase of MAPbI_3 emphasised the effect of the strength of the hydrogen-bonding on the octahedral tilting.⁴² Since it is well known that strong hydrogen bonding correlates with greater electronegativity of the acceptor atom, it is not surprising to find that the Young's modulus increases with anion electronegativity in the sequence $E_I < E_{Br} < E_{Cl}$ (Fig. 5 (c)).⁴³

It is pleasing to find that the trend in the Young's moduli of the MAPbX_3 phases correlates well with all the chemical factors that are expected to influence it. At the same time, however, this leads to an ambiguity because we are unable to ascertain which of the three factors has the greatest effect on the stiffness of the system. The three factors are to some extent interrelated (for example, they are all influenced by the anion size), but they are nevertheless distinct, and computational work will be necessary in order to shed light on their relative importance.

In addition to the elastic response, plastic deformation plays an important part in understanding the behaviour of materials under stress. We have therefore investigated another physical property, hardness, which is crucial for any industrial applications that might involve the MAPbX_3 perovskites. The hardness results from the combination of elastic and plastic deformations taking place in the vicinity of the nanoindenter tip.²⁷ Based on the Oliver and Pharr method, the hardness value was calculated by dividing the applied load (P) by the surface contact area developed under that load (A_c) (Fig. S2). It can clearly be seen in Fig. 3 that I-based perovskites require a much higher load to achieve the same displacement as their Br and Cl counterparts. Rather surprisingly, then, a trend of $H_I > H_{Br} > H_{Cl}$ has been observed, as shown in Table 1, with the Br- and Cl-based perovskites showing rather similar values. Since hardness is a measure of the dislocation interactions in the plastic zone in response to the induced pressure from the tip, I-based perovskites may show a higher hardness as a result of the lower symmetry of the structure. Multiple slip systems can be activated simultaneously to accommodate plastic flow for

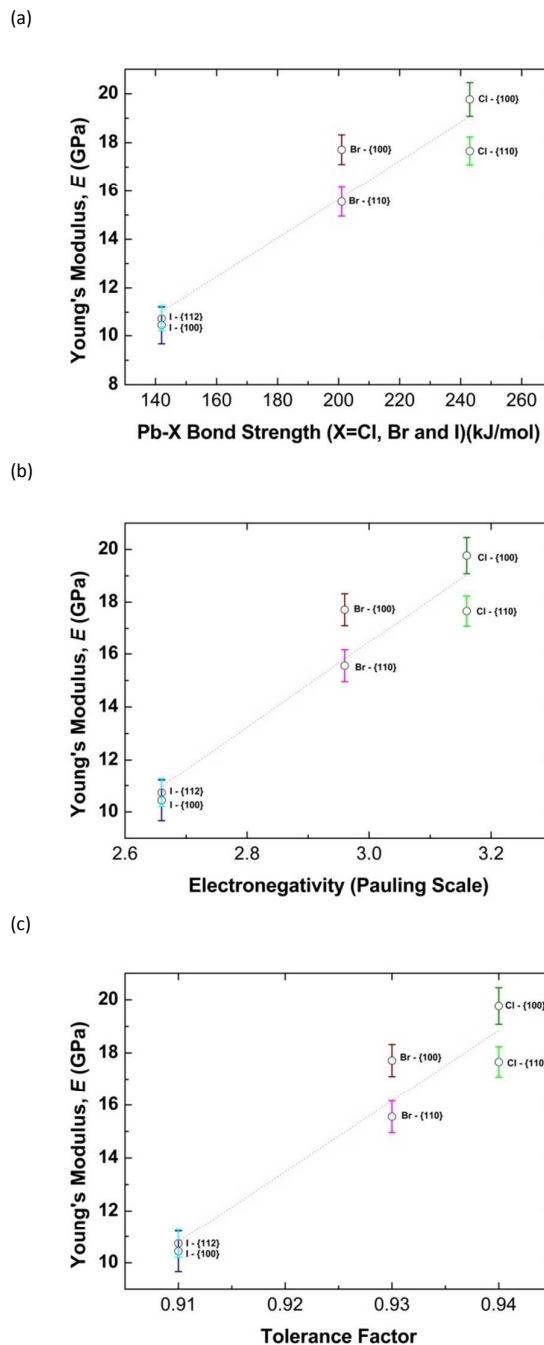


Fig. 5 Young's Modulus as a function of (a) Bond Strength³⁸ (b) Electronegativity⁴³ (c) Calculated tolerance factors⁴¹. All the three chemical factors point to the same direction, although it is challenging to estimate their relative importance (the red dotted lines are a guide to the eye to show the general trend).

high-symmetry cubic crystals, whereas fewer dislocation systems may be active in tetragonal systems.²² The high hardness and low elastic modulus of the I-based perovskites mean that, although it is the least resistant to elastic deformation, it is superior to its Br- and Cl-based counterparts in resisting plastic deformation. Regarding the hardness anisotropy between different crystallographic orientations of

the Cl and Br systems, it is less significant than the elastic anisotropy. However, it was observed that the facets having higher stiffness also tend to show greater hardness, reflecting the stronger bonding along particular crystallographic orientations.

Conclusions

In summary, we have used nanoindentation to investigate the mechanical properties of the amine halide perovskites $\text{CH}_3\text{NH}_3\text{PbX}_3$ ($\text{X} = \text{Cl}, \text{Br}, \text{I}$). The Elastic Moduli of $\text{CH}_3\text{NH}_3\text{PbX}_3$ decreases along the series $E_{\text{Cl}} > E_{\text{Br}} > E_{\text{I}}$ and we identified three chemical factors that influence this trend: (i) the strength of Pb-X bonds, (ii) the relative packing density and (iii) hydrogen bonding interactions. At this stage it is not clear which, if any, of these factors is more dominant, since they all show the anticipated trends with stiffness.

The hardness of $\text{CH}_3\text{NH}_3\text{PbX}_3$ single crystals show that iodide based lead perovskites are more resistant to permanent deformation and exhibit better elastic recovery. In particular, the superior elastic recovery facilitates application in devices that require a return to the original shape after stresses are removed. On the other hand the lower hardness of bromide and chloride based systems is interesting for flexible devices, for instance as soft absorption layer in thin film solar cells.

In the context of solar cell research, a knowledge of mechanical properties is of crucial importance and has significant influence on manufacturing processes, the design of the cells, and their specific applications. The study of the intrinsic mechanical properties of the $\text{CH}_3\text{NH}_3\text{PbX}_3$ perovskites therefore gives a unique insight into underlying structure-property relations and contributes to the future design of devices with tailored properties.

Acknowledgements

The authors would like to thank Professor Jin-Chong Tan and Professor Wei Li for stimulating discussions. SS is supported by the Cambridge Overseas Trust and GK is the holder of a postdoctoral fellowship granted by the Deutsche Forschungsgemeinschaft (<http://www.dfg.de/en/>), KI1879. In Singapore, this work was supported by the Energy Research Institute at Nanyang Technological University.

Notes and reference

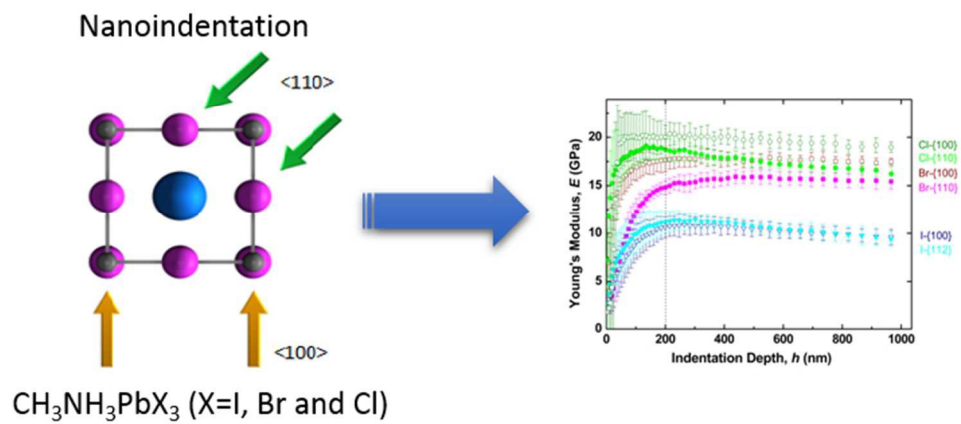
- 1 A. Kojima, K. Teshima, Y. Shirai and T. Miyasaka, *J. Am. Chem. Soc.*, 2009, **131**, 6050–6051.
- 2 M. A. Green, K. Emery, Y. Hishikawa, W. Warta and E. D. Dunlop, *Prog. Photovoltaics Res. Appl.*, 2015, **23**, 1–9.
- 3 M. Liu, M. B. Johnston and H. J. Snaith, *Nature*, 2013, **501**, 395–398.
- 4 H. J. Snaith, *J. Phys. Chem. Lett.*, 2013, **4**, 3623–3630.
- 5 H.-S. Kim, C.-R. Lee, J.-H. Im, K.-B. Lee, T. Moehl, A. Marchioro, S.-J. Moon, R. Humphry-Baker, J.-H. Yum, J. E. Moser, M. Grätzel and N.-G. Park, *Sci. Rep.*, 2012, **2**, 591.
- 6 M. He, D. Zheng, M. Wang, C. Lin and Z. Lin, *J. Mater. Chem. A*, 2014, **2**, 5994.

- 7 Y. Tidhar, E. Edri, H. Weissman, D. Zohar, G. Hodes, D. Cahen, B. Rybtchinski and S. Kirmayer, *J. Am. Chem. Soc.*, 2014, **136**, 13249–13256.
- 8 H. Zhou, Q. Chen, G. Li, S. Luo, T. -b. Song, H.-S. Duan, Z. Hong, J. You, Y. Liu and Y. Yang, *Science*, 2014, **345**, 542–546.
- 9 J. Burschka, N. Pellet, S.-J. Moon, R. Humphry-Baker, P. Gao, M. K. Nazeeruddin and M. Grätzel, *Nature*, 2013, **499**, 316–319.
- 10 M. Seetharaman, S. P. Nagarjuna, P. N. Kumar, S. P. Singh, M. Deepa and M. A. G. Namboothiry, *Phys. Chem. Chem. Phys.*, 2014, **16**, 24691–24696.
- 11 G. Xing, N. Mathews, S. S. Lim, N. Yantara, X. Liu, D. Sabba, M. Grätzel, S. Mhaisalkar and T. C. Sum, *Nat. Mater.*, 2014, **13**, 476–480.
- 12 P. Qin, S. Tanaka, S. Ito, N. Tetreault, K. Manabe, H. Nishino, M. K. Nazeeruddin and M. Grätzel, *Nat. Commun.*, 2014, **5**, 3834.
- 13 N. J. Jeon, J. H. Noh, Y. C. Kim, W. S. Yang, S. Ryu and S. Il Seok, *Nat. Mater.*, 2014, **13**, 897–903.
- 14 Y. He and G. Galli, *Chem. Mater.*, 2014, **26**, 5394–5400.
- 15 D. Shi, V. Adinolfi, R. Comin, M. Yuan, E. Alarousu, A. Buin, Y. Chen, S. Hoogland, A. Rothenberger, K. Katsiev, Y. Losovyj, X. Zhang, P. A. Dowben, O. F. Mohammed, E. H. Sargent and O. M. Bakr, *Science*, 2015, **347**, 519–522.
- 16 Q. Dong, Y. Fang, Y. Shao, P. Mulligan, J. Qiu, L. Cao and J. Huang, *Science*, 2015, **347**, 967–970.
- 17 G. Xing, N. Mathews, S. Sun, S. S. Lim, Y. M. Lam, M. Grätzel, S. Mhaisalkar and T. C. Sum, *Science*, 2013, **342**, 344–347.
- 18 S. A. Bretschneider, J. Weickert, J. A. Dorman and L. Schmidt-Mende, *APL Mater.*, 2014, **2**, 040701.
- 19 F. Deschler, M. Price, S. Pathak, L. E. Klintberg, D. Jarausch, R. Higler, S. Hu, T. Leijtens, S. D. Stranks, H. J. Snaith, M. Atatu, R. T. Phillips and R. H. Friend, *J. Phys. Chem. Lett.*, 2014, **5**, 1421–1426.
- 20 L. Dimesso, M. Dimamy, M. Hamburger and W. Jaegermann, *Chem. Mater.*, 2014, **26**, 6762–6770.
- 21 J. Feng, *APL Mater.*, 2014, **2**, 081801.
- 22 J. C. Tan and A. K. Cheetham, *Chem. Soc. Rev.*, 2011, **40**, 1059–80.
- 23 J.-C. Tan, P. Jain and A. K. Cheetham, *Dalton Trans.*, 2012, **41**, 3949–52.
- 24 W. Li, A. Thirumurugan, P. T. Barton, Z. Lin, S. Henke, H. H.-M. Yeung, M. T. Wharmby, E. G. Bithell, C. J. Howard and A. K. Cheetham, *J. Am. Chem. Soc.*, 2014, **136**, 7801–7804.
- 25 A. Poglitsch and D. Weber, *J. Chem. Phys.*, 1987, **87**, 6373.
- 26 B. R. Vincent, K. N. Robertson, T. S. Cameron and O. Knop, *Can. J. Chem.*, 1987, **65**, 1042–1046.
- 27 J. C. Tan, C. A. Merrill, J. B. Orton and A. K. Cheetham, *Acta Mater.*, 2009, **57**, 3481–3496.
- 28 W. Li, M. S. R. N. Kiran, J. L. Manson, J. A. Schlueter, A. Thirumurugan, U. Ramamurthy and A. K. Cheetham, *Chem. Commun.*, 2013, **49**, 4471–3.
- 29 J. C. Tan, T. D. Bennett and A. K. Cheetham, *Proc. Natl. Acad. Sci. U. S. A.*, 2010, **107**, 9938–43.
- 30 W. C. Oliver and G. M. Pharr, *J. Mater. Res.*, 1992, **7**, 1564–1583.
- 31 W. C. Oliver and G. M. Pharr, *J. Mater. Res.*, 2004, **19**, 3–20.
- 32 T. D. Bennett, J.-C. Tan, S. A. Moggach, R. Galvelis, C. Mellot-Draznieks, B. A. Reisner, A. Thirumurugan, D. R. Allan and A. K. Cheetham, *Chem. - A Eur. J.*, 2010, **16**, 10684–10690.
- 33 T. Baikie, Y. Fang, J. M. Kadro, M. Schreyer, F. Wei, S. G. Mhaisalkar, M. Graetzel and T. J. White, *J. Mater. Chem. A*, 2013, **1**, 5628.
- 34 C. C. Stoumpos, C. D. Malliakas and M. G. Kanatzidis, *Inorg. Chem.*, 2013, **52**, 9019–9038.
- 35 A. C. Fischer-Cripps, *Surf. Coatings Technol.*, 2006, **200**, 4153–4165.

ARTICLE

Journal Name

- 36 G. Giorgi, J.-I. Fujisawa, H. Segawa and K. Yamashita, *J. Phys. Chem. C*, 2014, **118**, 12176–12183.
- 37 A. Walsh, *J. Phys. Chem. C*, 2015, **119**, 5755–5760.
- 38 H. John, *Inorganic Chemistry Principles of Structure and Re Activity; 4th Edition; HarperCollinsColleg*, 1993., 1993.
- 39 V. M. Goldschmidt, *Naturwissenschaften*, 1926, **14**, 477–485.
- 40 R. D. Shannon, *Acta Crystallogr. Sect. A*, 1976, **32**, 751–767.
- 41 G. Kieslich, S. Sun and A. K. Cheetham, *Chem. Sci.*, 2014, **5**, 4712–4715.
- 42 J.-H. Lee, N. Bristowe, P. Bristowe and A. K. Cheetham, *Chem. Commun.*, 2015, **51**, 6434–6437.
- 43 L. Pauling, *The Nature of the Chemical Bond and the Structure of Molecules and Crystals: An Introduction to Modern Structural Chemistry*, Cornell University Press, USA, 3rd ed., 1960.



262x112mm (72 x 72 DPI)